


# Secondary electron yield of air-exposed ALD-$Al_2O_3$ coating on Ag-plated aluminum alloy

Xue-Man Wan(万雪曼), Tian-Cun Hu(胡天存), Jing Yang(杨晶), Na Zhang(张娜), Yun He(何鋆), and Wan-Zhao Cui(崔万照)

**Citation:**Chin. Phys. B, 2024, 33 (**11**): 113701. DOI: 10.1088/1674-1056/ad71b3
Journal homepage: http://cpb.iphy.ac.cn; http://iopscience.iop.org/cpb

**What follows is a list of articles you may be interested in**

---

## Quantum degenerate Bose-Fermi atomic gas mixture of $^{23}$Na and $^{40}$K

Ziliang Li(李子亮), Zhengyu Gu(顾正宇), Zhenlian Shi(师振莲), Pengjun Wang(王鹏军), and Jing Zhang(张靖)
Chin. Phys. B, 2023, 32 (**2**): 023701. DOI: 10.1088/1674-1056/aca14f

## Generation of high-energy-resolved $NH_3$ molecular beam by a Stark decelerator with 179 stages

Bin Wei(魏斌), Shunyong Hou(侯顺永), Hengjiao Guo(郭恒娇), Yabing Ji(纪亚兵), Shengqiang Li(李胜强), Jianping Yin(印建平)
Chin. Phys. B, 2019, 28 (**5**): 053701. DOI: 10.1088/1674-1056/28/5/053701

## Tuning the velocity and flux of a low-velocity intense source of cold atomic beam

Shu Chen(陈姝), Ying-Ying Li(李营营), Xue-Shu Yan(颜学术), Hong-Bo Xue(薛洪波), Yan-Ying Feng(冯焱颖)
Chin. Phys. B, 2017, 26 (**11**): 113703. DOI: 10.1088/1674-1056/26/11/113703

## Three-dimensional hexapole focusing of pulsed molecular beam for state selection

Yi Ke(柯毅), Xiao-Bing Deng(邓小兵), Zhong-Kun Hu(胡忠坤)
Chin. Phys. B, 2017, 26 (**8**): 083701. DOI: 10.1088/1674-1056/26/8/083701

## Intense source of cold cesium atoms based on a two-dimensional magneto-optical trap with independent axial cooling and pushing

Jia-Qiang Huang(黄家强), Xue-Shu Yan(颜学术), Chen-Fei Wu(吴晨菲), Jian-Wei Zhang(张建伟), Li-Jun Wang(王力军)
Chin. Phys. B, 2016, 25 (**6**): 063701. DOI: 10.1088/1674-1056/25/6/063701

---

# Secondary electron yield of air-exposed ALD-$Al_2O_3$ coating on Ag-plated aluminum alloy

Xue-Man Wan(万雪曼), Tian-Cun Hu(胡天存), Jing Yang(杨晶), Na Zhang(张娜), Yun He(何鋆), and Wan-Zhao Cui(崔万照)†

*National Key Laboratory of Science and Technology on Space Microwave, China Academy of Space Technology (Xi'an), Xi'an* 710100, *China*

(Received 3 June 2024; revised manuscript received 19 August 2024; accepted manuscript online 21 August 2024)

Secondary electron yield (SEY) of air-exposed metals tends to be increased because of air-formed oxide, hydrocarbon, and other contaminants. This enhances the possibility of secondary electron multipacting in high-power microwave systems, resulting in undesirable occurrence of discharge damage. $Al_2O_3$ coatings have been utilized as passive and protective layers on device packages to provide good environmental stability. We employed atomic layer deposition (ALD) to produce a series of uniform $Al_2O_3$ coatings with appropriate thickness on Ag-plated aluminum alloy. The secondary electron emission characteristics and their variations during air exposure were observed. The escape depth of secondary electron needs to exceed the coating thickness to some extent in order to demonstrate SEY of metallic substrates. Based on experimental and calculated results, the maximum SEY of Ag-plated aluminum alloy had been maintained at 2.45 over 90 days of exposure without obvious degradation by applying 1 nm $Al_2O_3$ coatings. In comparison, the peak SEY of untreated Ag-plated aluminum alloy grew from an initial 2.33 to 2.53, exceeding that of the 1 nm $Al_2O_3$ sample. The ultra-thin ALD-$Al_2O_3$ coating substantially enhanced the SEY stability of metal materials, with good implications for the environmental dependability of spacecraft microwave components.

**Keywords:** secondary electron yield (SEY), atomic layer deposition, air exposure, multipactor

**PACS:** 37.20.+j, 79.20.Hx, 68.37.–d **DOI:** 10.1088/1674-1056/ad71b3

## 1. Introduction

When primary electrons with a certain kinetic energy collide with the solid, a number of electrons are emitted from material surface, creating a variety of electronic signals, such as secondary electrons, backscattered electrons, photoelectrons, Auger electrons, and x-rays.[1–3] The phenomenon of secondary electron emission after electron bombardment has been extensively explored in the fields of microscopic analysis, photomultiplier tubes, microchannel plates, and multipacting effect.[4–8] For particle accelerators and high-power microwave components applications, the secondary electron yield (SEY) of interior surfaces plays a key role in the performance of electronic devices.[9] Under high radio frequency electromagnetic fields, it can even result in permanent surface damage and destruction due to electron-cloud effect, low pressure discharge, and multipacting effect.[10–12] Given that the penetration and escape depth of electron are both on the order of ten nanometers, SEY is particularly sensitive to primary electron incidence condition as well as material surface characteristics involving morphology, components, roughness, and atmospheric absorption.[13,14] One highly practical and efficient approach to resolving multipactor breakdown is to modulate SEY by applying specific film coatings on internal surface of devices.[15–17]

Ag-plated aluminum alloy is commonly utilized as a substrate material in space microwave components to lower electromagnetic loss during signal transmission. However, due to inevitable gas absorption and contamination from water vapor, dust, fluoride, sulfide, and other chemical substances that are adhered to or penetrated to metal surface during air exposure,[18–21] Ag plating properties will be negatively affected over several-months manufacturing and assembling phases of spacecrafts. The maximum SEY value ($\delta_{max}$) for Ag plating ranges from 1.97 to 2.50.[22] After being exposed to air environment for five years, $\delta_{max}$ ascends to 2.61,[20] indicating a decline in multipactor performance. Therefore, it is critical to understand how to preserve SEY performance of Ag plating while minimizing surface adsorption, oxidation, and contamination effect.

The atomic layer deposition (ALD) process is an innovative technology based on sequential, self-limiting surface reactions that allows for accurate fabrication of nanometer and sub-nanometer films by regulating the number of reaction cycles.[23] In contrast to physical vapor deposition and other chemical vapor deposition, ALD produces films that are less contaminated with carbon, oxygen, chlorine, and have good conformity in ultrahigh aspect ratio. In particular, ALD-$Al_2O_3$ coatings have been utilized as passive and protective layers on device packages to provide good environmental stability.[24] $Al_2O_3$ thin films demonstrate a stable environmental performance with SEY ranging from 2.9 to 4.08.[13] Xie *et al.*[25] reported that $Al_2O_3$ nanofilm stabilized SEY by inhibiting

†Corresponding author. E-mail: cuiwanzhao@126.com

© 2024 Chinese Physical Society and IOP Publishing Ltd 

aluminum alloy oxidation. After a year of storage, $\delta_{max}$ of 3 nm ALD-$Al_2O_3$ coating on aluminum alloy remained at 2.9. Wang *et al.*[26] and Lian *et al.*,[27] respectively, proposed to grow 1 nm $Al_2O_3$ protective layer on MgO film to prevent MgO from deliquescing into $Mg_2(OH)_2CO_3$ and $MgCO_3$, which would impair SEY performance. Good SEY environmental stability is exhibited by $Al_2O_3$ protective layer that can sustain SEY levels over time without obvious deliquescence.

In consideration of the stable environmental property of $Al_2O_3$, it is worth studying an appropriate thickness of protective $Al_2O_3$ layer to minimize air-exposure induced damage of metals without bringing obvious changes in SEY. We applied thermal ALD technology to fabricate different coating thickness of $Al_2O_3$ on Ag-plated aluminum alloy and the SEY values under air-exposure storage were investigated. The current study revealed that ALD-$Al_2O_3$ coatings in the nanoscale range can inhibit SEY deterioration of Ag plating, suggesting a potential approach to preventing multipactor effect by suppression ascending of SEY.

## 2. Materials and methods

The deposition of $Al_2O_3$ coatings was carried out by thermal ALD method on phosphor-doped conductive polished Si wafers (n-type Si, crystal direction $\langle 100 \rangle$) for microstructure characterization and on Ag-plated aluminum for SEY measurements.

### 2.1. Preparation of ALD-$Al_2O_3$ coatings

ALD-$Al_2O_3$ coatings were deposited from thermal ALD process. The chemical reaction is described by

$$\mathrm{Al{-}OH^{*} + Al(CH_3)_3 \rightarrow Al{-}O{-}Al(CH_3)_2^{*} + CH_4}, \quad (1)$$

$$\mathrm{Al{-}O{-}Al(CH_3)_2^{*} + 2H_2O \rightarrow Al{-}O{-}Al(OH)_2^{*} + 2CH_4}, \quad (2)$$

and the total reaction is given by

$$\mathrm{2Al(CH_3)_3 + 3H_2O \rightarrow Al_2O_3 + 6CH_4}. \quad (3)$$

$Al(CH_3)_3$ (trimethylaluminum or TMA) and $H_2O$ were utilized as precursors for $Al^{3+}$ and $O^{2-}$, respectively, and $N_2$ was employed as both carrier gas and purge gas. The chemical reactant sources and $N_2$ purge gas were maintained at 22 °C. Each gas was introduced into the reaction chamber in the sequence of TMA pulse for 0.1 s, $N_2$ purge for 10 s, $H_2O$ pulse for 0.3 s, and another $N_2$ purge for 10 s. Prior to the deposition, Si wafers and Ag substrates were ultrasonically cleaned in acetone and alcohol for 20 min, respectively. Subsequently, substrates were placed in the reaction chamber at 300 °C and heated for a duration of 30 min prior to the reaction. Table 1 lists deposition parameters used in this study. The count of ALD cycles is specified as 5, 10, 25, 50, 100, 200, and 300, accordingly.

**Table 1.** Deposition settings for ALD-$Al_2O_3$ process.

| Substrate | Si (100) and Ag-plated aluminum |
|---|---|
| $N_2$ pressure (MPa) | 0.3 |
| Flow rate (sccm) | TMA (40); $H_2O$ (40) |
| Reactant temperature (°C) | 22 |
| Pulse time (s) | TMA (0.1)/$N_2$ (10)/ $H_2O$ (0.3)/$N_2$ (10) |
| Deposition temperature (°C) | 300 |
| Deposition rate (Å/cycle) | 1 |

### 2.2. Microstructure characterization of ALD-$Al_2O_3$ coatings

A spectroscopic ellipsometer (M-2000, J. A. Woollam, USA) was used to analyze film thickness and uniformity of ALD-$Al_2O_3$ coatings. Atomic force microscopy (AFM, Bruker Dimension ICON, Germany) and scanning electron microscopy (SEM, Zeiss Gemini 300, Germany) were carried out to examine the surface morphology. The investigation of element distribution and impurity content was conducted in energy dispersive spectroscopy (EDS, Bruker XFlash, Germany) and x-ray photoelectron spectroscopy (XPS, PSP CTX400, UK) tests. The penetration depth measured by EDS analysis is generally above 1 μm, while that of XPS is generally within 10 nm. Consequently, in order to exclude the impact of substrate signals, the EDS test is primarily used to define the element distribution over the surface, and XPS analysis is utilized to characterize the chemical composition of the film.

### 2.3. SEY measurements of ALD-$Al_2O_3$ coatings

SEY measurements for $Al_2O_3$ coatings have been performed by the pulse-beam method specialized for dielectrics to avoid surface charging. The measurement facility depicted in Fig. 1(a) was built by our research group, relying on a hemispherical collector system and electron gun (STAIB Instruments, Germany) in the range of 30 eV–30 keV conducting in ultrahigh vacuum at $6\times10^{-8}$ Pa. To improve secondary electron yield accuracy, electron collector modules are equipped with a three-layer grid and a single collector. The signal generator (HAMEG HM8150, Germany) delivers square pulses of 6 μs duration with total incident charges of $1.9\times10^{-12}$ C at primary electron energy of 300 eV, and the electron beam density is approximately $2.4\times10^{-12}$ C/mm$^2$. The pulse signal is amplified into a fast current amplifier (DHPCA-100, FEMTO, Germany) at $10^6$ V/A, and then received and displayed by the oscilloscope (RIGOL DS1054, China). SEY ($\delta$) of ALD-$Al_2O_3$ coatings can be delivered by

$$\delta = \frac{I_{\text{first grid}} + I_{\text{second grid}} + I_{\text{third grid}} + I_{\text{collecter}}}{I_{\text{sample stage}} + I_{\text{first grid}} + I_{\text{second grid}} + I_{\text{third grid}} + I_{\text{collecter}}} = \frac{I_{\text{SE,tot}}}{I_{\text{p}}}. \quad (4)$$

SEY measurements do not make a distinction of elastic back-scattering current, inelastic backscattering current and

true secondary electron current having kinetic energies below 50 eV. We define the total secondary electron emission current from the surface as $I_{\mathrm{SE,tot}}$ which is the sum of $I_{\mathrm{first\ grid}}$, $I_{\mathrm{second\ grid}}$, $I_{\mathrm{third\ grid}}$, and $I_{\mathrm{collector}}$. $I_{\mathrm{p}}$ represents the vertical incident primary electron current obtained by connecting sample stage ($I_{\mathrm{sample\ stage}}$), grids ($I_{\mathrm{first\ grid}}+I_{\mathrm{second\ grid}}+I_{\mathrm{third\ grid}}$), and collector ($I_{\mathrm{collector}}$) together.

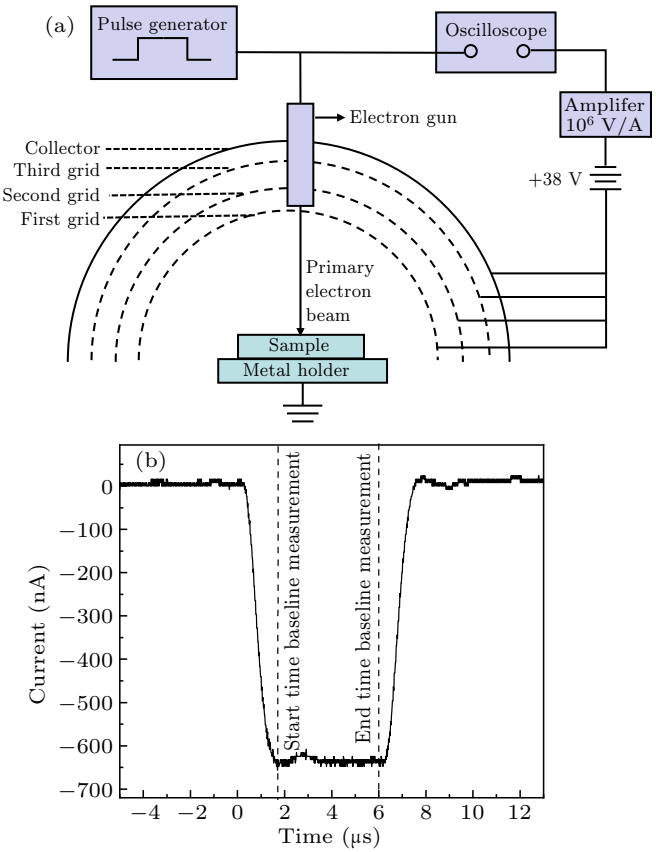



**Fig. 1.** (a) Schematic overview of SEY measurement, (b) total secondary electron current at primary electron energy of 300 eV from 0.5 nm ALD-$Al_2O_3$ coating on Ag-plated substrate. The vertical dashed lines indicated the pulse window where the baseline was measured.

In our experimental conditions, the trapped positive charges within the dielectric film are unable to create a sufficient electric field or surface potential that would induce variations in secondary electron trajectory by taking into account the following steps:

(i) To reduce the surface charging occurred in per pulse, the irradiation pulse time was set as 6 μs with small electron beam density of $2.4\times10^{-12}$ C/mm$^2$.

(ii) The secondary electron would pass through three-layer grid before reaching the collector, which decreases the number of the electrons. To overcome ternary electron emission and grid transmission loss, the total secondary electron current $I_{\mathrm{SE,tot}}$ was measured at +38 V biased collector connected with three-layer grids. The metallic sample stage is grounded to discharge and to prevent the primary electron energy from being varied by charging effect for each of primary energy points.

(iii) The deposited substrate is Ag-plated aluminum alloy, while sample holder and sample stage are made of molybdenum and 304 stainless steel, respectively. The surface charging effect could be compensated during the pulse duration, ensuring the sample potential was set to 0 V.

Figure 1(b) shows the secondary electron current signal. The signal baseline that is estimated to be constant corresponds with $I_{\mathrm{SE,tot}}$. As indicated by the stable current, the magnitude of secondary electron emission has not been impacted by electrostatic field.

## 3. Results and discussion

### 3.1. Surface microstructure characterization of ALD-$Al_2O_3$ coatings

The ALD method is self-limiting, successive surface reactions wherein a single atomic layer thickness is deposited per cycle.[28–30] Surface saturation of precursors results in a constant thin-film growth rate, and the number of deposition cycles determines the film thickness. Therefore, coating thickness and the number of reaction cycles are supposed to be proportional. Spectroscopic ellipsometry was employed to analyze 50, 100, 200, and 300 cycles films on Si substrate to determine whether the deposition behaved as a typical ALD growth mode. As shown in Fig. 2, the growth thickness has a linear ratio to deposition cycles of roughly 1 Å/cycle, and the coating thickness is around 5 nm, 10 nm, 20 nm, 30 nm. The film uniformity ($\mu$) was estimated using

$$\mu = (T_{\mathrm{max}} - T_{\mathrm{min}})/(2\times T_{\mathrm{average}})\times 100\%, \tag{5}$$

where $T_{\mathrm{max}}$ is the maximum value of the coating thickness, $T_{\mathrm{min}}$ is the minimum value of the coating thickness and $T_{\mathrm{average}}$ is the average value of the coating thickness. The results are presented in Table 2. The homogeneous layer indicates that the chemical reaction between precursors and substrate gradually reaches saturation. The less uniformity of 50 cycles film as compared to other samples might be attributed to that oxide films on Si wafers affect refractive index of materials. It is also possible that the formation of small island nucleation on substrate during the pre-film growth period has a large impact on optical parameters, resulting in a deviation from the fitted data.

**Table 2.** ALD-$Al_2O_3$ coatings thickness and uniformity at different deposition cycles.

| Deposition cycles | Thickness (nm) | Uniformity (%) |
|---|---|---|
| 50 | 4.61 | 7.48 |
| 100 | 9.42 | 4.14 |
| 200 | 19.57 | 3.40 |
| 300 | 29.84 | 4.27 |

The average surface roughness of 5 nm, 10 nm, 20 nm, and 30 nm samples determined by AFM analysis is 0.18 nm,

0.17 nm, 0.15 nm, and 0.18 nm, respectively, as shown in Fig. 3. It is observed that as the film was initially formed parallel to the substrate, surface roughness exhibits a decreased trend with the increase of coating thickness. The minimal roughness of 0.15 nm is obtained in 20 nm sample. When the thickness reaches 30 nm stacked with more $Al_2O_3$ monolayers, $Al_2O_3$ islands emerge following a transition from 2D planar growth to 3D island growth, and the surface roughness increases to 0.18 nm. The good density, homogeneity, and compactness of ALD-$Al_2O_3$ coatings are confirmed by AFM measurements.

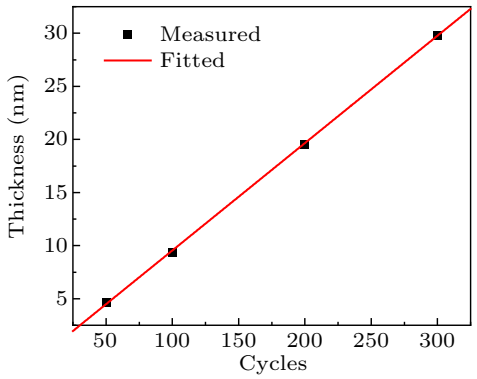



**Fig. 2.** The relationship between growth thickness and deposition cycle.

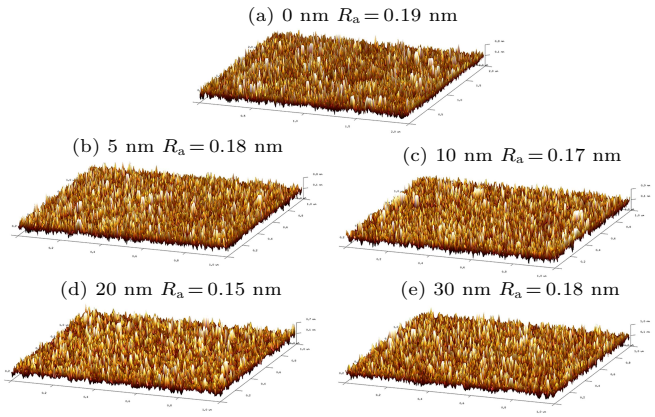



**Fig. 3.** AFM three-dimensional maps of ALD-$Al_2O_3$ coatings on Si.

X-ray photoelectron is an effective way to detect the chemical composition of thin films while excluding the substrate signal. XPS tests were performed on 0 nm, 0.5 nm, 1 nm, 2.5 nm, and 5 nm ALD-$Al_2O_3$ coatings on Ag plating, as illustrated in Fig. 4(a). There is an Al 2p characteristic peak indicating the presence of Al element. EDS mappings obtained from 30 nm ALD-$Al_2O_3$ coating further confirm the homogeneous distribution of Al element over the surface (Fig. 5). As the film thickness grows, the typical peak of the matrix Ag progressively diminishes, and 5 nm film sample is primarily made up of Al and O components. The characteristic peak strength is used to estimate the photoelectron counts of Al 2p and O 1s, and the atomic ratio of O to Al element ($\beta_{O:Al}$) is shown in Fig. 4(b). It could be inferred from gradually stabilized $\beta_{O:Al}$ that the density and compactness of ALD-$Al_2O_3$ coatings is supposed to be stabilized with the deposition thickness.

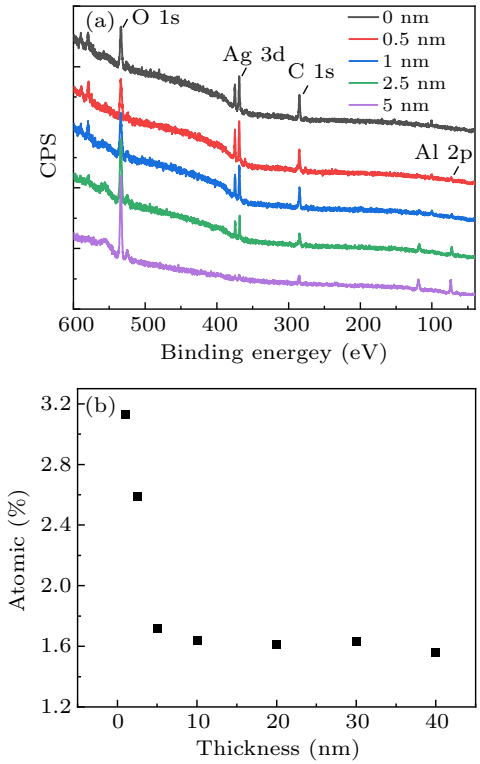



**Fig. 4.** (a) XPS spectra and (b) the atomic ratio $\beta_{O:Al}$ of ALD-$Al_2O_3$ coatings.

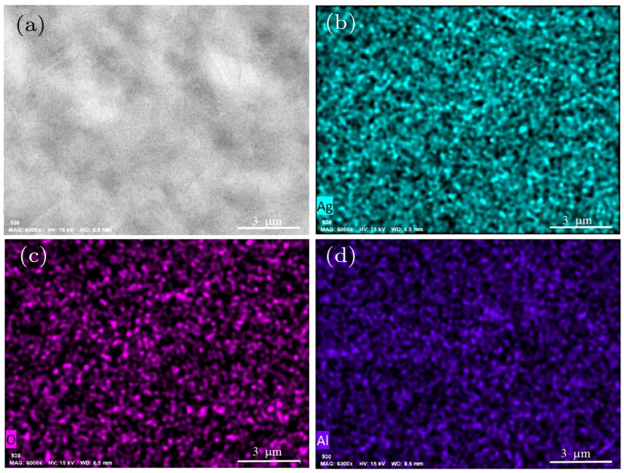



**Fig. 5.** (a) SEM image and (b)–(d) EDS maps of 30 nm ALD-$Al_2O_3$ coating.

### 3.2. SEY characterization of ALD-$Al_2O_3$ coatings

A series of 0 nm, 0.5 nm, 1 nm, 2.5 nm, and 5 nm thick ALD-$Al_2O_3$ coatings on Ag-plated substrate are subjected to SEY measurements after air exposure, as seen in Fig. 6. SEY characteristics of ALD-$Al_2O_3$ coatings deposited on Ag plating are correlated with both the bottom substrate and the top coating. The peak value of SEY coefficients gradually rises from 2.25 to 3.82 as the ALD-$Al_2O_3$ coating thickness increases from 0.5 nm to 5 nm, as shown in Fig. 6(a). SEY curves of the composite layered structure are comparable to those of the as-received Ag-plated substrate. The emission

yield is determined by the electron penetration depth $R$ and escape depth $X_s$, which are associated with the primary electron energy $E_p$.[31] When the SEY reaches its maximum value, at the energy of $E = E_{pm}$, the largest primary electron penetration depth $R_{pm}$ and secondary electron escape depth $X_s$ are calculated through

$$R = 1.15 \times 10^2 \times E_p^{1.35}/\sigma, \tag{6}$$

$$X_s = 50.4 \times E_{pm}^{1.35}/\sigma, \tag{7}$$

where $E_p$ is primary electron incident energy, $E_{pm}$ is the primary electron energy at $\delta_{max}$ and $\sigma$ is the density of the materials (3.96 g/cm$^3$ for $Al_2O_3$). The results are listed in Table 3.

**Table 3.** The electron penetration depth $R$ and escape depth $X_s$ at $E_p = E_{pm}$ of $Al_2O_3$.

| Thickness (nm) | $R_{pm}$ (nm) | $X_s$ (nm) |
|---|---|---|
| 0.5 | 3.76 | 1.64 |
| 1 | 4.71 | 2.06 |
| 2.5 | 6.76 | 2.96 |
| 5 | 7.86 | 3.44 |

The $Al_2O_3$ coatings play a major effect on SEY characterization in the ALD-$Al_2O_3$ composite layered structure. At relatively low $E_p$, where $R < X_s$, internal secondary electrons only emit from the top coating. Incident electrons of $E_p =$ 0.1 keV have a penetration depth of approximately 1.3 nm. There is no discernible difference in SEY between 2.5 nm and 5 nm samples because secondary electron emission is exclusively provided by the top $Al_2O_3$ layer. If $E_p$ rises, more primary electrons collide with materials, increasing the possibility of internal electron emission, resulting in an ascending phase of the SEY curve. At $E_p = E_{pm}$ where $\delta = \delta_{max}$, primary electron penetrates through the top ALD-$Al_2O_3$ coating and interact with the bottom Ag plating substrate. SEY is co-excited by both ALD-$Al_2O_3$ coating and Ag plating. At $E_p > E_{pm}$, more internal secondary electrons are created along the incident range, but it is hard for most of the electrons to overcome energy loss during collisions as well as vacuum–solid interface because of large penetration depth, causing a decline in SEY curve with higher incident energy.

In addition, the first crossover energy $E_{c1}$ at $\delta = 1$ is an important parameter for multipactor threshold as well as surface potential, which could either result in negative or positive states depending on whether SEY is lower or greater than 1. If the material being irradiated is electrically isolated from ground, then negative charges would be accumulated due to more electrons injected into materials than those emitted, when $\delta$ is lower than 1 at $E_p < E_{c1}$ in the region of a few tens of eV. Unfortunately, this point cannot be studied through SEY measurements because of the poor visibility of the primary electron beam and the difficulty in focusing the electron beam when the required primary energies are below 100 eV. For $\delta_{max} > 1$, the $E_{c1}$ could be analytically expressed as[32]

$$E_{c1} = 0.51 E_{pm} \delta_{max}^{-1.32}. \tag{8}$$

Since the $\delta_{max}$ of ALD-$Al_2O_3$ coating is 3.7–4.08,[33–36] the thicker $Al_2O_3$ coatings, the more secondary electrons are ejected from the surface layer, leading to an increased SEY of the composited structure. By applying a passivation layer to reduce metal oxidation and contamination, the thickness of oxide coating is designed to be less than primary electron penetration depth to avoid an increasing multipactor risk. As previously stated, if the coating thickness exceeds $R = 1.3$ nm, electrons cannot penetrate through the top layer and reach the bottom substrate at low energy levels ($E_p = 0.1$ keV). The 2.5 nm coated sample has larger SEY data than 0.5 nm and 1 nm coated samples, which happens because all of the secondary electrons of the 2.5 nm sample are emitted from $Al_2O_3$ layer at $E_p = 0.1$ keV. In addition, it is observed from Fig. 6(a) that SEY of 0.5 nm $Al_2O_3$ coating is a little lower than that of the Ag-plated substrate (0 nm sample). This may be attributed to a reduction in impurities on the sample surfaces.[37] Prior to ALD deposition, substrates were cleaned in an ultrasonic bath with acetone, alcohol, and DI water in sequence for 20 min each, which permits surface contaminants and chemicals to be partially removed under organic cleaning. In addition, substrates were pre-heated at 300 °C for 30 min before the start of the coating procedure. The reduction in hydrocarbon contamination and the thermal desorption of $H_2O$ may have contributed to a decrease in SEY under the action of heat energy.

The effect of air exposure on SEY of ALD-$Al_2O_3$ coatings was studied, and SEY characterization was re-performed after air exposure for 30 days and 90 days stored in the drying cabinet, respectively. The results are presented in Figs. 6(b)–6(d). The shift of higher SEY is typical for contaminated surfaces. Both the bare Ag plating and the 0.5 nm ALD-$Al_2O_3$ coating exhibit a comparable SEY pattern as incident energy increases. Over a 90-day exposure period, $\delta_{max}$ of the Ag plating sample (0 nm sample) gradually climbed from 2.33 to 2.53, while $\delta_{max}$ of the 0.5 nm ALD-$Al_2O_3$ coating grew from 2.35 to 2.46 (Table 4). Due to partial oxidation and poor homogeneity, the sub-nanometer oxide film has a minor inhibitory influence on SEY deterioration. According to Table 4, when the coating thickness exceeds 1 nm, $\delta_{max}$ essentially stabilizes at its initial value during the exposure period. Considering that the secondary electron emission coefficient mainly contributes to top $Al_2O_3$ coatings for 2.5 nm and 5 nm samples, SEY is higher than that of uncoated metal, which is undesirable in high-frequency RF devices. Although 1 nm ALD-$Al_2O_3$ coating initially increases SEY of Ag plating, $\delta_{max}$ of Ag plating grew to a similar level as 1 nm coated sample under 30 days of exposure. After 90 days exposure, $\delta_{max}$ of the Ag plating exceeds that of 1 nm coated sample. It is proposed that the nanometer-scale, compact, and uniform ALD-$Al_2O_3$ coatings significantly improve the stability of SEY by preventing oxidation and atmospheric pollution. An ALD-$Al_2O_3$ coating of 1 nm was the optimum protective layer thickness for preventing SEY deterioration and enhancing SEY environmental stability of metal materials exposed to long-term duration.

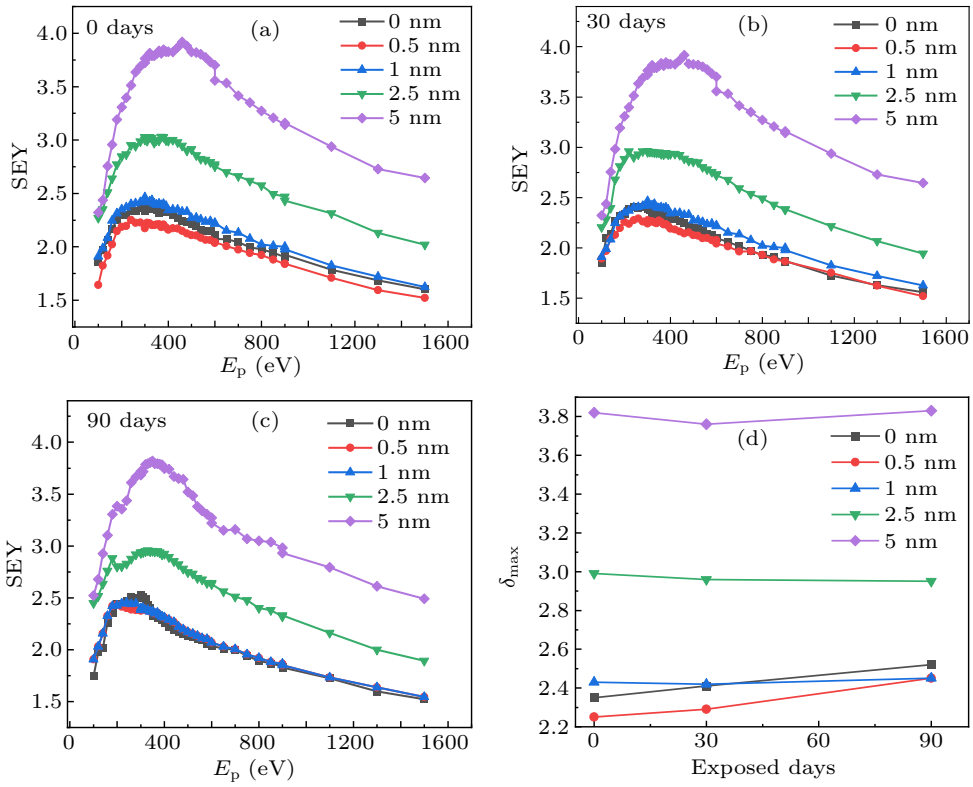



**Fig. 6.** (a)–(c) SEY curve as a function of primary electron energy of ALD-$Al_2O_3$ coatings air-exposed for 90 days, (d) the variation of $\delta_{max}$ of ALD-$Al_2O_3$ coatings.

**Table 4.** The $\delta_{max}$ and $E_{pm}$ of ALD coated samples in air-exposure duration time.

| Thickness (nm) | 0 day | | 90 days | |
|---|---|---|---|---|
| | $\delta_{max}$ | $E_{pm}$ (keV) | $\delta_{max}$ | $E_{pm}$ (keV) |
| 0 | 2.33 | 0.30 | 2.53 | 0.26 |
| 0.5 | 2.25 | 0.28 | 2.46 | 0.26 |
| 1 | 2.43 | 0.30 | 2.45 | 0.28 |
| 2.5 | 2.99 | 0.34 | 2.95 | 0.34 |
| 5 | 3.82 | 0.38 | 3.81 | 0.38 |

## 4. Conclusion

In this work, the ALD technique has been utilized to fabricate a series thickness of $Al_2O_3$ coating on Ag-plated aluminum alloy. The impact of oxide film and air exposure on SEY characteristics was investigated. The results show that SEY of uncoated sample increased from 2.33 to 2.53 after 90 days of storage in dry air. A compact and homogeneous film with good environmental stability of SEY is obtained when the thickness of $Al_2O_3$ coating on Ag plating surface is more than 1 nm, maintaining the original condition of $\delta_{max}$. However, growing the amount of $Al_2O_3$ coating monolayers decreases the Ag substrate's participation in the secondary electron emission process, leading to an increase in SEY. For the purpose of minimizing SEY variations of Ag-plated aluminum alloy on the exposure duration and preserving metal SEY properties to a large extent, the optimum thickness of $Al_2O_3$ coating is supposed to be 1 nm, which is less than the primary electron penetration depth and the secondary electron escape depth. This controllable, ultra-thin ALD-$Al_2O_3$ coating provides an effective method to suppress the secondary electron emission deterioration of active metals and nitride materials, which is critical for resolving multipactor problem in space microwave components.

## Acknowledgements

Project supported by the Sustainedly Supported Foundation by National Key Laboratory of Science and Technology on Space Microwave (Grant No. HTKJ2023KL504001) and the National Natural Science Foundation of China (Grant No. 62101434).

## References

[1] Kang Y F, Li B, Zhao J Y, Ge B Z, Weng M, Shi Z Q and Zhao Y Q 2020 *Vacuum* **172** 109043
[2] Greenblatt M H 1949 *Rev. Sci. Instrum.* **20** 646
[3] Powell C J and Seah M P 1990 *J. Vac. Sci. Technol. A* **8** 735
[4] Wiza J L 1979 *Nucl. Instrum. Meth.* **162** 587
[5] Jokela S J, Veryovkin I V, Zinovev A V, Elam J W, Peng, Q, Mane A U, McDaniel F D and Doyle B L 2011 *AIP Conf. Proc.* **1336** 208
[6] Bishop H E and Riviere J C 1969 *J. Appl. Phys.* **40** 1740
[7] Seiler H 1983 *J. Appl. Phys.* **54** R1
[8] Hueso J, Raboso D, Schmitt D, Boria V E, Martinez B and Vicente C 2011 *IEEE Tran. Electron. Dev.* **58** 3205
[9] Zhang Y T, Yang J, Yang Z L, Miao G H, Zhang N and Cui W Z 2024 *Rare Metal Mat. Eng.* **53** 465 (in Chinese)
[10] Song Q, Cui W Z, Yang J and Hu T C 2019 *Chin. Space Sci. Technol.* **39** 43 (in Chinese)
[11] Zhang N, Cui W Z and Wang X B 2011 *Space Electronic Technol.* **8** 38 (in Chinese)
[12] Nistor V, González L A, Aguilera L, Montero I, Galán L, Wochner U and Raboso D 2014 *Appl. Surf. Sci.* **315** 445

[13] Tao S X, Chan H W and Van D G H 2016 *Materials* **9** 1017
[14] Sattler J M, Coutu R A, Lake R, Laurvick T, Back T and Fairchild S 2017 *J. Appl. Phys.* **122** 055304
[15] Jin X L, Ji P, Zhuge L J, Wu X M and Jin C G 2022 *Chin. Phys. B* **31** 27901
[16] Wang F, Zhao Q, Li J, Wang K, Huang Z and Cui W 2018 *Coatings* **8** 249
[17] Feng G B, Li Y, Li X J, Xie G B and Liu L 2022 *Chin. Phys. B* **31** 107901
[18] He Y, Shen T, Wang Q, Miao G H, Bai C J, Yu B, Yang J, Feng G B, Hu T C, Wang X B and Cui W Z 2020 *Appl. Surf. Sci.* **520** 146320
[19] Wang J, Taaj S, Valizadeh R, Wang Y and Wang S 2018 *IEEE Trans. Nucl. Sci.* **65** 2620
[20] Wang D, Cai Y H, He Y, Xu Y N and Jia Q Q 2022 *Res. Phys.* **33** 105231
[21] Gineste T, Belhaj M, Teyssedre G and Puech J 2015 *Appl. Surf. Sci.* **359** 398
[22] Hu T, Zhu S, Zhao Y, Sun X, Yang J, He Y, Wang X, Bai C, Bai H and Wei H 2022 *Chin. Phys. B* **31** 047901
[23] Parsons G N, George S M and Knez M 2011 *MRS Bull.* **36** 865
[24] Gougousi T 2016 *Prog. Cryst. Growth Charact.* **62** 1
[25] Xie G, Bai H, Miao G H, Feng G B, Yang J, He Y, Li X J and Li Y 2021 *Nanomaterials* **11** 3282
[26] Wang Y, Yan B, Wen K, Liu S, Qi M, Zhang B, Gu J and Yao W 2021 *Nanoscale Res. Lett.* **16** 1
[27] Lian Z, Zhu X, Wang D, Meng X and He Y 2024 *J. Phys. D: Appl. Phys.* **57** 125302
[28] Burton B B, Lavoie A R and George S M 2008 *J. Electrochem. Soc.* **155** D508
[29] Feng Z, Wang Y, Hao J, Jing M, Lu F, Wang W, Cheng Y, Wang S, Liu H and Dong H 2022 *Chin. Phys. B* **31** 057701
[30] Yang H, Chen W, Li M Y, Xiong F, Wang G, Zhang S, Deng C Y, Peng G and Qin Q S 2020 *Chin. Phys. Lett.* **37** 076801
[31] Young J R 1956 *J. Appl. Phys.* **27** 14
[32] Dionne G F 1975 *J. Appl. Phys.* **46** 3347
[33] Chan H W, Prodanović V, Theulings A, Hagen C W, Sarro P M and Graaf H V D 2021 *J. Instrum.* **16** P07024
[34] Cao W, Wang B, Yang Y, Zhu B, Guo J, Xu P, Bai X, Qin J, Wang C, Zhu J and Bai Y 2021 *Ceram. Int.* **47** 9866
[35] Guo J J, Wang D, Xu Y T, Zhu X P, Wen K L, Miao G H, Cao W W, Si J H, Lu M and Guo H T 2019 *AIP Adv.* **9** 095303
[36] Wei W, Yan B, Heng Y, Liu S, Zhang B, Peng H, Wang Y and Wen K 2023 *J. Instrum.* **18** P02002
[37] Yang Z, Wang X, Chen Z, Wang R and Cui W Z 2024 *Space Sci. Technol.* **4** 0108